**Journal of Electrical Engineering, Electronics, Control and Computer Science – JEEECCS, Volume 8, Issue 27, pages 43-54, 2022**

# Fuzzy sliding mode control of a shunt active power filter for harmonic reduction in grid-connected photovoltaic systems

Réné Constant Fanjip[1], Serge Raoul Dzonde Naoussi[2], Charles Hubert Kom[1,3], Arnaud Nanfak[3], Gildas Martial Ngaleu[3]

[1]Laboratory of Computer Science Engineering and Automation
Higher Technical Teachers Training College of Douala, University of Douala, Cameroon

[2]Laboratory of Technology and Applied Sciences, University Institute of Technology, University of Douala, Cameroon

[3]Laboratory of Energy, Materials, Modelling and Methods
National Higher Polytechnic School of Douala, University of Douala, Cameroon

rene_constant1@yahoo.fr, serge.dzonde@univ-douala.com, Charleshurbert.kom@gmail.com, nanfak.arnaud@yahoo.fr, gmngaleu@yahoo.fr

***Abstract*** **– This paper deals with harmonic reduction in a grid-connected photovoltaic system using an active shunt power filter (SAPF). For this purpose, a fuzzy sliding mode control (Fuzzy-SMC) is proposed for SAPF control. In the proposed controller, the dynamics parameters of sliding mode controller (SMC) are determined by the fuzzy logic controller (FLC). The SMC is based on a sliding plane and no longer requires the discontinuous component of the classical SMC. The results obtained by the computer simulations carried out by MATLAB/Simulink software are compared with those obtained with hysteresis and sliding mode controls. In the case where the power of the PV generator is higher than that of the load, the load is supplied by the PV generator and the surplus energy is injected into the grid. After connection of the filter, the current supplying to the load goes from a THD of 22.33% to 0.29% with the proposed controller, compared to the 0.98% obtained with the SMC or the 0.95% obtained with the hysteresis. In the case where the power of the PV generator is lower than that of the load, the load is fed by both the grid and the PV generator. The current obtained after filtering has a THD of 2.77% with the proposed controller.**

***Keywords-Grid-connected PV system, SAPF, Fuzzy-SMC, Harmonics mitigation***

## I. Introduction

The use of renewable energy is in continuous evolution nowadays due to the fossil fuel depletion and the necessity to reduce their negative impact on the planet. The photovoltaic production of energy is increasingly being implemented in urban and rural areas as they are free-noise, easily available and low-cost. In rural communities, the distribution of electrical energy is generally organized into microgrids [1]. These microgrids can be divided in two categories, standalone microgrids and grid-connected ones.

In standalone photovoltaic microgrids, the solar power plant is disconnected from the grid. In this case, the plant is designed for a low voltage distribution network and is subject to voltage imbalance during an increasing of load imbalance that may be dangerous for some equipment such as 3-phase motors [2]. Moreover, standalone PV system cannot supply load during night and some times during the day due to bad weather conditions; therefore, an energy storage system is conventionally used in order to stabilize the level of produced energy [3].For over a decade, several studies have resulted in scientific publications on the analysis of standalone PV systems. As solar power plant produces DC voltage, an inverter is always used for the continuous voltage to alternative voltage. In [4], the authors propose a three-phase four-leg voltage sourced inverter as a solution to load unbalance in a standalone network. They show that this configuration, including its control algorithm, improve power quality of the microgrid. Raseenaet al. [5] works on the reduction of number of conversion stages in the PV to load connection by the integration of DC-DC converter with multilevel inverter. That leads to an efficient and reliable system. In [6], Himaliet al presents a review that analyses several configurations of PV arrays associated to their power conditioning system including inverter and DC-DC converter.

In grid-connected microgrid, the solar power plant is used to support the grid in case of load increasing. This interconnection must satisfy the standard requirements in terms of voltage amplitude, period and current harmonics [7]. A phase lock loop (PLL) is used for the control of the inverter in order to synchronize both sources. Instead of the inverter, the plant needs sometimes battery chargers (including DC-DC converter) and switched mode power supplies. All these power electronic converters, act as internal nonlinear dynamic loads view from the AC-current supply side. Add to this, there are external nonlinear loads such as speed control drivers, arc furnaces, voltage regulators, un interruptible power supply connected to the grid. All these nonlinear loads will inject harmonic currents at the AC source side of the interconnected grid [8].That will cause several harmful effects, including electromagnetic interference, different types of distortion for the current and voltage signals, overheating of the different power system devices and worsen power factor correction (PFC) performances [8]-[9]. A large number of standards are strictly associated with the level of current THD allowed in a network. Adak and al. [10] investigate on the impact of solar irradiation and ambient temperature on total harmonic distortion of the current in a solar power plant. The results show that input current THD of nonlinear load increase in low irradiation.

Two main configurations are present in the literature to solve the power quality problem in grid-connected PV systems. The first configuration is to use an active filter independently of the PV system. In this configuration, the PV system is a source in its own right like the grid and performs two functions, namely supplying loads and injecting currents into the grid when weather conditions allow it. An active filter is used to eliminate harmonics produced by non-linear loads. In the second configuration the PV system is directly associated with the active filter and performs three functions, namely supplying the loads, injecting to the grid and solving power quality problems. This article deals with the first configuration. In this configuration the passive LC filters are used to eliminate the harmonics produced by the grid connection inverter [11].There are different configurations of passive filter such as single tuned, double-tuned and band-pass. Theoretically LC passive filters eliminate harmonics by showing zero impedance at the selected frequency [12], but their weakness is the fact that they can eliminate only the harmonic component of inverter and not the harmonics produced by the non-linear loads in the system. To eliminate harmonics produced by non-linear loads, shunt active power filter (SAPF) then appears as the most reliable instrument. It performs by first detecting all the harmonic currents contained in the current wave, and then, generates and injects corrective mitigation current back into the power system to cancel out all the detected harmonic currents [13]. The performances of the parallel active filter depend on the reference current extraction algorithm, the control strategy, the inverter structure, the modulation technique used to generate the control signals applied to the power switches and the control of the DC bus. The harmonic current extraction algorithm is the central element that conditions the performance of the SAPF. Indeed, an accurate and efficient harmonics extraction leads to proper and fast reference current generation which further controls the SAPF to generate the required injection current for harmonics mitigation [14]. Several harmonic current extraction techniques exist in the literature such as the instantaneous PQ theory [14]-[15], the neural identification technique [16], the synchronous reference frame theory [17] or the triangle orthogonal principle [18] in the time-based domain and the discrete Fourier transform [19], the fast Fourier transform [20] or the recursive discrete Fourier transform [21] in the frequency-based domain. Boum et al. [22] proposed a Sliding mode controller for SAPF control. Many other such as $H_{infini}$ controller [23], hysteresis controller [24], PI controller [25], fuzzy logic controller [26], and predictive current controller [27] can be found in the literature. Few studies have been presented in the literature on harmonic mitigation of grid-connected PV systems using shunt active filter. In [28], a new technique employing Kalman filter estimator is used for improve the performance of SAPF in term of overall harmonic reduction and power factor is proposed for grid-connected PV system. In this study, the KF estimator is used to replace the common low-pass filter technique in d-q algorithm. The authors of [29] proposes a three-phase voltage fed type shunt active filter system based on hysteresis current control to eliminate harmonic generation due to nonlinear loads towards a grid-connected PV system. In [30], the harmonics due to the inverter circuit and non-linear load are eliminated using SAPF in PV system connected to grid. The hysteresis control method is used and different operating conditions have been simulated.

This paper presents the design of fuzzy sliding mode control (Fuzzy-SMC) of a shunt active power filter for harmonic reduction in grid-connected PV system. In this paper, the instantaneous PQ theory is used for the identification of harmonic currents. A fuzzy-SMC is used for the SAPF control.

After the introduction section, the remaining part of this paper is organized as follows: the multi-source system is presented in section 2. The section 3 is devoted to SAPF description. Simulation results and discussion are done in section 4 and section 5 conclude the paper.

## II. MULTI-SOURCE DESCRIPTION

The multi-source system of this work is a PV generator connected to the grid network. In Fig. 1, the functional components are presented.

Figure 1. Grid-connected PV structure

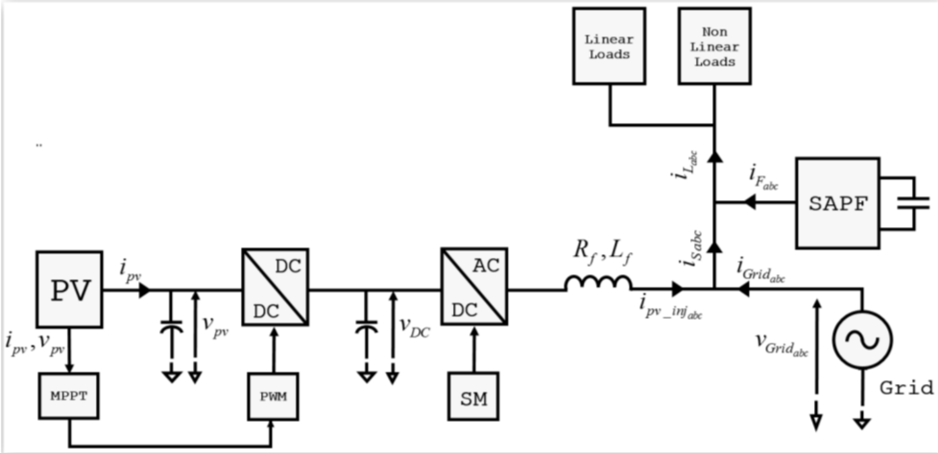


### A. Modelling of PV Array

The solar cell is the basic unit of a PV panel and it is the element in charge of transforming the sun rays or photons directly into electric power by a process called "photovoltaic effect" [31]. The Fig. 2 shows the equivalent circuit of solar cell and Eq. 1 the expression of output current of solar cell.

Figure 2. Equivalent circuit of solar cell [31]

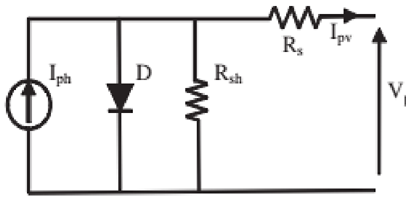


$$I_{pv} = I_{ph} - I_s\left(\exp\left(\frac{q\left(V_{pv}+R_sI_{pv}\right)}{nK_bT}\right)-1\right) - \frac{V_{pv}+R_sI_{pv}}{R_{sh}} \quad (1)$$

with

$$I_{ph} = \left(\frac{G}{G_r}\right)\left(I_{scr}+k_i\left(T-T_r\right)\right)$$

$$I_s = I_{rs}\left(\frac{T}{T_r}\right)^3 \exp\left(\frac{qE_g}{nK_b}\left(\frac{1}{T_r}-\frac{1}{T}\right)\right)$$

$$I_{rs} = \frac{I_{scr}}{\exp\left(\frac{qV_{oc}}{nK_bT}\right)-1}$$

where $I_{pv}$ is output current of PV cell $(A)$; $I_{ph}$ is photocurrent $(A)$; $I_D$ is diode current $(A)$; $V_{pv}$ is output voltage of PV cell $(V)$; $G$ is solar irradiation $(W/m^2)$; $G_r$ is solar irradiation in SRC conditions $(W/m^2)$; $T$ is cell temperature $(°C)$; $T_r$ is cell temperature in SRC conditions $(°C)$; $k_i$ is temperature coefficient of short-circuit $(A/K)$; $I_{scr}$ is short-circuit current of PV module at SCR conditions $(A)$; $I_S$ is diode saturation current $(A)$; $q = 1.602\times10^{-19}\,J/\mathrm{V}$ is electronic charge; $n$ is diode ideality factor; $K_b = 1.381\times10^{-23}\,J/K$ is Boltzmann's gas constant; $I_{rs}$ is diode saturation current at $T_r\ (A)$ and $E_g = 1.602\times10^{-19}\,J/\mathrm{V}$ is Activation energy of saturation current.

For $N_S$ cells in series and $N_P$ cells in parallel, the characteristic equation of a PV module is delivered as below:

$$I_{pv} = N_PI_{ph} - N_PI_s\left(\exp\left(\frac{q\left(V_{pv}+R_sI_{pv}\right)}{N_SnK_bT}\right)-1\right) - \frac{V_{pv}+R_sI_{pv}}{R_{sh}} \quad (2)$$

### B. Adaptation stage and MPPT algorithm

The adaptation stage of the PV panel voltage represented in Fig. 3 is a boost DC-DC converter. The Boost converter is widely used for this application due to its simple circuitry, system design, high conversion efficiency and low voltage stress [32]. It is necessary step to allow a PV generator to produce the maximum persistent power, at any value of the metrological terms or loads variations.

Figure 3. DC-DC boost converter structure

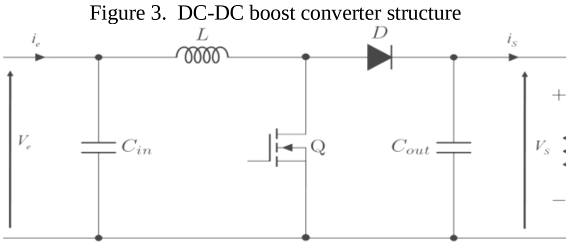


The boost converter is controlled by a maximum power extraction technique call Maximum Power Point Tracking (MPPT) Technique. Several MPPT technics have been proposed in literature such as perturb and observe (P&O) [32], Incremental conductance (INC) [33], fuzzy logic [34] or neutral network [35]. The Fig. 4 presents the flow chart of P&O MPPT algorithm used in this work. Indeed P&O algorithm is probably the most frequently and robust used in practice due to its easy implementation. In the implementation of this algorithm, the voltage $V_{PV}(n)$ and the current $I_{PV}(n)$ are measured to calculate the power $P_{PV}(n)$ of PV generator. The variations of power $\Delta P_{PV} = P_{PV}(n) - P_{PV}(n-1)$ and voltage $\Delta V_{PV} = V_{PV}(n) - V_{PV}(n-1)$ are calculated. The following value of the duty cycle $\alpha(n+1)$ returned by the MPPT algorithm is such that:

$$\begin{cases} if \quad \Delta P_{PV} \times \Delta V_{PV} > 0, \quad \alpha(n+1) = \alpha(n) + \Delta\alpha \\ if \quad \Delta P_{PV} \times \Delta V_{PV} < 0, \quad \alpha(n+1) = \alpha(n) - \Delta\alpha \end{cases} \tag{3}$$

where $\Delta\alpha$ is duty cycle increment value.

### C. Synchronization Method

Due to increasing demand of energy and depletion of fossil fuel reserves, the sources of renewable energy such as solar, wind, hydro geothermal and biomass are getting popular. The interconnection of renewable energy sources to the grid through inverters has become essential. The use of grid connected inverters is justified by the continuous nature of the renewable power produced and the need to inject clean energy into the grid [7, 36]. Several synchronization methods have been proposed in literature and can be classified as time-based domain or frequency-based domain including Time zero crossing detection, Kalman Filter, discrete Fourier transform, nonlinear least square, adaptive notch filtering, artificial intelligence, delayed signal cancellation, phase locked loop, and frequency locked loop [37].

Figure 4. Flow chart of P&O MPPT algorithm [31]

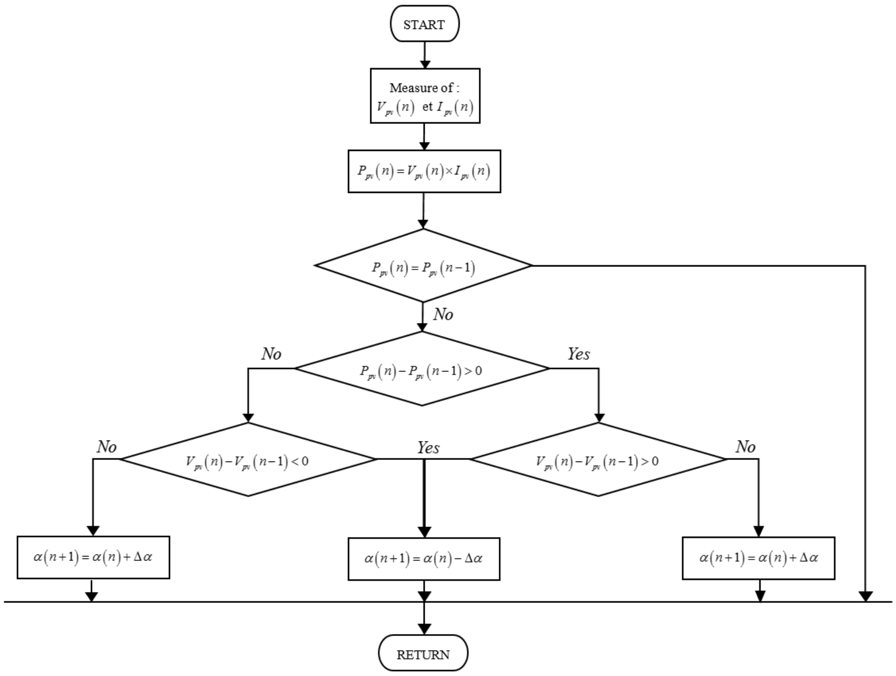


The synchronization method used in this paper is presented in Fig. 5. It is a current-controlled inverter where the reference current $i_q^*$ is set to zero and reference current $i_d^*$ is computed by the control loop of the DC link.

## III. SAPF DESCRIPTION

Defined as the sinusoidal components of a periodic signal, having frequencies multiple of the fundamental wave, harmonics cause serious problems to loads connected to the network, such as heating problems, unexpected resonances, disturbances in electronic equipment, "logic" faults in digital circuits, malfunctioning of motors, generators and degradation of the power factor [37, 38]. One of the solutions used to solve the harmonic problem is the use of active parallel filters. Connected in parallel to the grid, active parallel filters compensate for current harmonics by injecting an equal but opposite phase harmonic current [14]. Fig. 6 shows the schematic diagram of the SAPF operating principle.

### A. Power Part

The power part contains a voltage source inverter (VSI), the coupling filter and an energy storage system connected through the DC link [39]. The VSI is a two-level inverter with 6 bi-directional power switches in current. This part synthesises the compensation currents that are previously calculated by the control part.

### B. Control Part

The control part of the SAPF contains the harmonic identification and compensation current calculation block and the control strategy block used to generate the VSI control signals. The identification method used in this paper is the instantaneous PQ theory method and the controller used is a Fuzzy-SMC.

Figure 5. Block diagram of synchronization method used

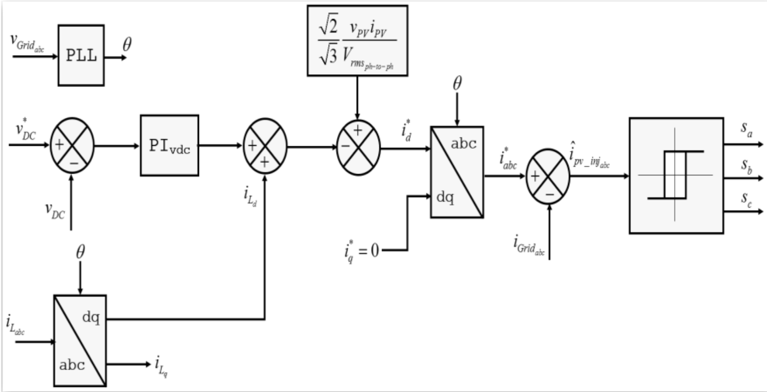


Figure 6. Operating principle of SAPF

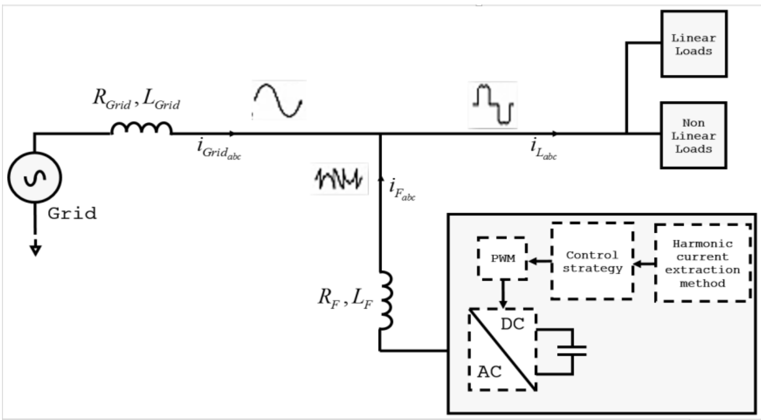


*1) Instantaneaous PQ theory*

The instantaneous active and reactive power theory or PQ theory introduced by H. Akagi at 1983, is a time-based method, which is used to avoid difficulties dueto the high number of calculations whenimplementing frequency-based methods.It transforms the fundamental component of the signal into a DC component and the harmonic components into AC components. The principle of the harmonic current identification method consists in eliminating the DC component from the instantaneous active and reactive powers [40]. This method is based on the Concordia transformation of simple grid voltages given in Eq. 4 and load line currents given in Eq. 5.

$$\begin{bmatrix} v_{S\alpha} \\ v_{S\beta} \end{bmatrix} = \sqrt{\frac{2}{3}} \begin{bmatrix} 1 & -\frac{1}{2} & -\frac{1}{2} \\ 0 & \frac{\sqrt{3}}{2} & -\frac{\sqrt{3}}{2} \end{bmatrix} \begin{bmatrix} v_{Grid_a} \\ v_{Grid_b} \\ v_{Grid_c} \end{bmatrix} \tag{4}$$

$$\begin{bmatrix} i_{L\alpha} \\ i_{L\beta} \end{bmatrix} = \sqrt{\frac{2}{3}} \begin{bmatrix} 1 & -\frac{1}{2} & -\frac{1}{2} \\ 0 & \frac{\sqrt{3}}{2} & -\frac{\sqrt{3}}{2} \end{bmatrix} \begin{bmatrix} i_{La} \\ i_{Lc} \\ i_{Lc} \end{bmatrix} \tag{5}$$

Where $(v_{S\alpha}, v_{S\beta})$ are the components of the grid voltage in Concordia reference frame and $(i_{L\alpha}, i_{L\beta})$ are the components of the load currentin the Concordia reference frame.

the real and imaginary powers are given by:

$$\begin{bmatrix} p_{inst} \\ q_{inst} \end{bmatrix} = \begin{bmatrix} v_{S\alpha} & v_{S\beta} \\ -v_{S\beta} & v_{S\alpha} \end{bmatrix} \begin{bmatrix} i_{L\alpha} \\ i_{L\beta} \end{bmatrix} \tag{6}$$

where $p_{inst}$ is the real instantaneous power and $q_{inst}$ is the imaginary instantaneous power.

As the harmonics are linked to the AC components of the instantaneous powers, the harmonic currents that represent the identified currents, called reference currents in the Concordia reference frame, are given by:

$$\begin{bmatrix} i_{Comp\alpha} \\ i_{Comp\beta} \end{bmatrix} = \frac{1}{v_{S\alpha}^2 + v_{S\beta}^2} \begin{bmatrix} v_{S\alpha} & -v_{S\beta} \\ v_{S\beta} & v_{S\alpha} \end{bmatrix} \begin{bmatrix} \tilde{p}_{inst} \\ \tilde{q}_{inst} \end{bmatrix} \tag{7}$$

where $\tilde{p}_{inst}$ is the AC component of instantaneous real power, $\tilde{q}_{inst}$ is the AC component of instantaneous imaginary power and $\left(i_{Comp\alpha}, i_{Comp\beta}\right)$ are the components of reference currents in the Concordia reference frame.

These AC components of instantaneous power are obtained using a low-pass filter (LPF) or a high-pass filter (HPF) as shown in Fig. 7.

Figure 7. Filters for extracting alternative components
a. High-pass filter b. Low-pass filter

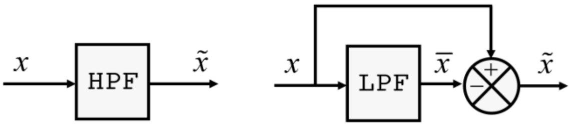


The inverse Concordia transform applied to the compensation currents in the stationary reference frame allows to have the three-phase reference currents given by:

$$\begin{bmatrix} i_{Compa} \\ i_{Compb} \\ i_{Compc} \end{bmatrix} = \sqrt{\frac{2}{3}} \begin{bmatrix} 1 & 0 \\ -\frac{1}{2} & \frac{\sqrt{3}}{2} \\ -\frac{1}{2} & -\frac{\sqrt{3}}{2} \end{bmatrix} \begin{bmatrix} i_{Comp\alpha} \\ i_{Comp\beta} \end{bmatrix} \tag{8}$$

Where $\left(i_{Compa}, i_{Compb}, i_{Compc}\right)$ are the components of three-phase reference currents.

*2) Control strategy*

In the indirect or voltage control strategy the harmonic currents identified in the load current are compared with those injected by the SAPF and a controller adjusts the control of the power switches according to the current error [41]. The control strategy used in this paper is a Fuzzy-SMC where the parameters of the sliding mode control law are determined by a fuzzy logic controller (FLC).

The SMC is based on the non-linear model of the filter given in the three-phase reference frame by:

$$\begin{cases} L_F \dfrac{di_{Fa}}{dt} = -R_F i_{Fa} + v_{Fa} - v_{Grida} \\ L_F \dfrac{di_{Fb}}{dt} = -R_F i_{Fb} + v_{Fb} - v_{Gridb} \\ L_F \dfrac{di_{Fc}}{dt} = -R_F i_{Fc} + v_{Fc} - v_{Gridc} \end{cases} \tag{9}$$

By applying the direct Concordia transform to the SAPF model given in Eq. (9), the SAPF model in the stationary frame is given by:

$$\begin{cases} L_F \dfrac{di_{F\alpha}}{dt} = -R_F i_{F\alpha} + v_{F\alpha} - v_{Grid\alpha} \\ L_F \dfrac{di_{F\beta}}{dt} = -R_F i_{F\beta} + v_{F\beta} - v_{Grid\beta} \end{cases} \tag{10}$$

with

$$\begin{bmatrix} v_{F\alpha} \\ v_{F\beta} \end{bmatrix} = \sqrt{\frac{2}{3}} \begin{bmatrix} 1 & -\frac{1}{2} & -\frac{1}{2} \\ 0 & \frac{\sqrt{3}}{2} & -\frac{\sqrt{3}}{2} \end{bmatrix} \begin{bmatrix} v_{Fa} \\ v_{Fb} \\ v_{Fc} \end{bmatrix}$$

$$\begin{bmatrix} i_{F\alpha} \\ i_{F\beta} \end{bmatrix} = \sqrt{\frac{2}{3}} \begin{bmatrix} 1 & -\frac{1}{2} & -\frac{1}{2} \\ 0 & \frac{\sqrt{3}}{2} & -\frac{\sqrt{3}}{2} \end{bmatrix} \begin{bmatrix} i_{Fa} \\ i_{Fb} \\ i_{Fc} \end{bmatrix}$$

As one variable corresponds to one controller, the stationary filter model is used for controller synthesis. Recent advances have made it possible to solve the chattering problem caused by the discontinuous part of the control law by using a sliding plane instead of a sliding surface.

The sliding planes chosen for the currents $i_{F\alpha}$ and $i_{F\beta}$ are given by:

$$\begin{cases} P\left(i_{F\alpha}\right) = k_1 e\left(i_{F\alpha}\right) + k_2 \int e\left(i_{F\alpha}\right) \\ P\left(i_{F\beta}\right) = k_3 e\left(i_{F\beta}\right) + k_4 \int e\left(i_{F\beta}\right) \end{cases} \tag{11}$$

where $e\left(i_{F\alpha}\right) = i_{Comp\alpha} - i_{F\alpha}$ is the tracking error of the variable $i_{F\alpha}$ , $e\left(i_{F\beta}\right) = i_{Comp\beta} - i_{F\beta}$ is the tracking error of the variable $i_{F\beta}$ and $k_1$ , $k_2$ , $k_3$ and $k_4$ positive constants.

The control laws are determined so that they verify the relations of Eq. (12) during the slip mode.

$$\begin{cases} P\left(i_{F\alpha,\beta}\right) = 0 \\ \dfrac{d}{dt} P\left(i_{F\alpha,\beta}\right) = 0 \end{cases} \tag{12}$$

By applying the conditions of Eq. (12) to the sliding planes of Eq. (11), the control laws are given by:

$$\begin{cases} v_{F\alpha\_ref} = \dfrac{k_2}{k_1} L_F e\left(i_{F\alpha}\right) + v_{Grid\alpha} + R_F i_{F\alpha} + L_F \dfrac{di_{Comp\alpha}}{dt} \\ v_{F\beta\_ref} = \dfrac{k_4}{k_3} L_F e\left(i_{F\beta}\right) + v_{Grid\beta} + R_F i_{F\beta} + L_F \dfrac{di_{Comp\beta}}{dt} \end{cases} \tag{13}$$

The idea of the controller proposed in this paper is to determine the constants $k_1$ , $k_2$ , $k_3$ and $k_4$ by a fuzzy controller in order to build a dynamic sliding mode controller. Fig.8 shows the structure of the controller proposed.

The fuzzy part ofproposed controller is based on Mamdani type fuzzy inference mechanism. It receives as input the tracking error and the derivative of the tracking error of the variables $i_{F\alpha}$ et $i_{F\beta}$ and returns as output the controller constants of the SMC. The structure of FLC is shown in Fig. 9. Deterministic input variables are transformed into linguistic input variables in the fuzzification step. Then based on the fuzzy rules and the linguistic input variables, a decision is made by exploiting approximate reasoning.The output linguistic variables are obtained at the end of this step. Defuzzification, which is thelast step, transforms the linguistic output variables into deterministic output variables [42].

Figure 8. Bloc diagram of proposed controller

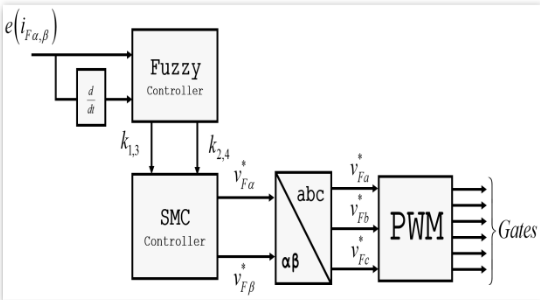


Figure 9. Bloc diagram of FLC [42]

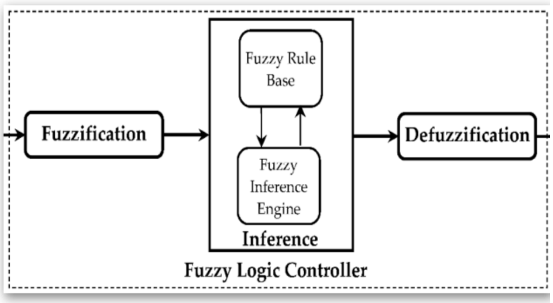


Fuzzification is done by defining membership functions (MFs) for each of the deterministic input variables. The notations used to represent the MFs of the tracking errors are Big Negative (BN), Small Negative (SN), Zero (Z), Small Positive (SP), Big Positive (BP). The notations used to represent the MFs of the tracking error derivatives are Negative (N), Zero (Z), Positive (P). based on experience and practice, the parameters of all FMs are determined. The Fig. 10 and 11 show these MFs. For tracking errors, triangular functions are used for the SN, Z and SP MFs, and trapezoidal functions for the BN and BP MFs. For the derivatives of the tracking errors, triangular functions are used for all MFs.

Figure 10. Membership functions of $e(i_{F\alpha})$ and $e(i_{F\beta})$

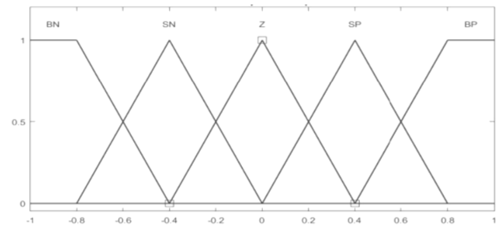


Figure 11. Membership functions of $\frac{de(i_{F\alpha})}{dt}$ and $\frac{de(i_{F\beta})}{dt}$

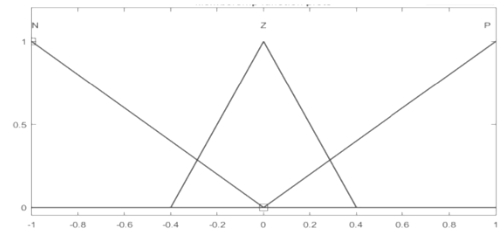


The defuzzification is done by defining MFs for each of the output linguistic variables. The centroid methodis used for defuzzification. The notations used to represent the output MFs are Big Negative (BN), Small Negative (SN), Zero (Z), Small Positive (SP), Big Positive (BP). The triangular functions are used for all MFs. The Fig. 12 shows these MFs.

Figure 12. Membership functions of $\frac{k_2}{k_1}$ and $\frac{k_4}{k_3}$

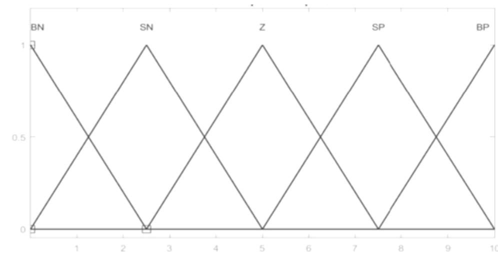


Based on heuristics, the rules are selected for the FLC to generate each output. The "and" connection is used to connect the both inputs. The fuzzy rules are listed in Table I.

TABLE I. FUZZY RULES

| $de(i_{F\alpha,\beta})/dt$ \ $e(i_{F\alpha,\beta})$ | ***BN*** | ***SN*** | ***Z*** | ***SP*** | ***BP*** |
|---|---|---|---|---|---|
| ***N*** | PG | PG | PM | PM | NG |
| ***Z*** | PG | PM | Z | NM | NG |
| ***P*** | PM | PM | NG | NG | NM |

## IV. SIMULATION RESULTS AND DISCUSSION

After the presentation of the system elements and the synthesis of the proposed control law for the active filter, this section presents the simulation results performed with MATLAB/Simulink software. Two operating scenarios will be simulated and the results obtained will be compared with those obtained with hysteresis and sliding mode correctors. The different operating scenarios will be carried out by varying the power of the load and the climatic conditions.The PV source parameters, Boost converter parameters, P&O MPPT algorithm parameters and grid parameters are given in TableII, III, IV and V respectively. The other simulation parameters are given in Table VI.

TABLE II. PV SOURCE PARAMETERS

| *Name* | *Parameters* | *Values* | *unity* |
|---|---|---|---|
| *Cells per module* | $N_{Cell}$ | 60 | |
| *Maximum power* | $P_m$ | 218.871 | *W* |
| *Voltage at PPM* | $V_{MPP}$ | 29.3 | *V* |
| *Current at PPM* | $I_{MPP}$ | 7.47 | *A* |
| *Open circuit voltage* | $V_{OC}$ | 36.6 | *V* |
| *Short-circuit current* | $I_{SC}$ | 7.97 | *A* |
| *Diode ideality factor* | $n$ | 0.98928 | |
| *Shunt resistance* | $R_{Sh}$ | 350.2415 | Ω |
| *Series resistance* | $R_S$ | 0.38174 | Ω |
| *Panel in series* | $N_S$ | 17 | |
| *Panel in parallel* | $N_P$ | 9 | |

TABLE III. BOOST CONVERTER PARAMETERS

| *Name* | *Parameters* | *Values* | *unity* |
|---|---|---|---|
| *Inductance* | $L$ | 4.5 | *mH* |
| *Input filter capacitance* | $C_e$ | 10 | $\mu F$ |
| *Output filter capacitance* | $C_S$ | 5000 | $\mu F$ |

TABLE IV. P&O MPPT PARAMETERS

| *Name* | *Parameters* | *Values* |
|---|---|---|
| *Initial duty cycle* | $\alpha_{init}$ | 0.2 |
| *Maximum duty cycle* | $\alpha_{\max}$ | 1 |
| *Minimum duty cycle* | $\alpha_{\min}$ | 0.01 |
| *Increment value* | $\Delta\alpha$ | 0.0001 |

TABLE V. GRID PARAMETERS

| *Name* | *Parameters* | *Values* | *unity* |
|---|---|---|---|
| *Frequency* | $f_{Grid}$ | 50 | *Hz* |
| *Phase-to-phase voltage* | $V_{rms_{ph-to-ph}}$ | 400 | *V* |
| *Grid resistance* | $R_{Grid}$ | 0.1 | Ω |
| *Grid Inductance* | $L_{Grid}$ | 0.15 | *mH* |

TABLE VI. OTHERS PARAMETERS

| *Name* | *Parameters* | *Values* | *unity* |
|---|---|---|---|
| *SAPF resistance* | $R_F$ | 1 | *m*Ω |
| *SAPF Inductance* | $L_F$ | 23 | *mH* |
| *DC/AC capacitances* | $C_1 = C_2$ | 40 | $\mu F$ |
| *SAPF Reference DC power* | $v_{DC}^*$ | 800 | *V* |
| *SM Reference DC power* | $v_{DC}^*$ | 800 | *V* |
| *MPPT PWM frequency* | $f_{PWM}$ | 10 | *kHz* |
| *SAPF PWM frequency* | $f_{PWM}$ | 15 | *kHz* |

### A. $P_{Load} < P_{pv}$

This scenario corresponds to the case where the power of the load is lower than that of the PV generator. The values of solar radiation and module temperature used are:

$$G = 1000W/m^2 \text{ and } T = 25°C \tag{13}$$

The simulation is done over 0.5 seconds with the SAPF connected at 0.1 seconds. Fig. 11, shows the waveforms of the PV generator current, the grid current and the resultant current $i_{Sabc}(t)$. Fig.12 shows the waveforms of the load and SAPF currents. Fig.13 shows the THD of the PV generator, grid, resultant and load currents.

As the power of the PV generator is higher than the power of the load, there is an injection of additional power to the grid. This observation is illustrated in the curves in Fig. 11 where the PV generator current and the grid current are in phase opposition. The resulting current $i_{Sabc}(t)$, which is the PV generator current minus the grid current, is equivalent to the current drawn by the load. The non-linear nature of the load causes the waveform to be distorted up to 0.1 seconds, the time corresponding to the connection of the SAPF. The connection of the filter results in the injection of harmonic currents identical to those contained in the load current, but of opposite phase. An improvement in the shape of the resulting current $i_{Sabc}(t)$ is observed, reducing its THD from 22.33% to 0.29% with the fuzzy-SMC control compared to 0.99 obtained with the hysteresis control and 1.01 obtained with the sliding mode control. The action of SAPF allows to have a better quality current injected to the grid with a THD of 0.93%.

Table VII shows the THD of the panel current, the grid current and the resulting current $i_{Sabc}(t)$ before and after filtering obtained with the hysteresis, SMC and fuzzy-SMC correctors.

TABLE VII. COMPARISON WITH SMC AND HYTHERESIS CONTROLLERS

| | | *Hysteresis* | *SMC* | *Fuzzy-SMC* |
|---|---|---|---|---|
| ***THD before filter*** | $i_{pv}$ | 3 | 3 | 3 |
| | $i_{Grid}$ | 1.01 | 1.01 | 1.01 |
| | $i_S$ | 22.33 | 22.33 | 22.33 |
| ***THD after filter*** | $i_{pv}$ | 0.83 | 0.83 | 0.80 |
| | $i_{Grid}$ | 0.93 | 0.93 | 0.93 |
| | $i_S$ | 0.95 | 0.98 | 0.29 |

### B. $P_{Load} > P_{pv}$

This scenario corresponds to the case where the power of the load is higher than the power of the PV generator. The values of solar irradiation and module temperature used are:

$$G = 400W/m^2 \text{ and } T = 45°C \tag{14}$$

The simulation is done over 0.5 seconds with the SAPF connected at 0.1 seconds. Fig. 14, shows the waveforms of the PV generator current, the grid current and the resultant current $i_{Sabc}(t)$. Fig. 15 shows the waveforms of the load and SAPF currents. Fig. 16

shows the THD of the PV generator, grid, resultant and load currents.

As the power of the PV generator is lower than that of the load, there is an additional power input from the grid. This observation is made on the curves in Fig. 14 where the PV generator and grid currents are in phase. The resulting current $i_{Sabc}(t)$, which is the sum of the PV generator and grid currents, is equivalent to the current drawn by the load. The non-linear nature of the load causes the waveform to be distorted up to 0.1 seconds, the time corresponding to the connection of the active filter. The connection of the SAPF leads to the injection of harmonic currents identical to those contained in the load current, but of opposite phase. An improvement in the shape of the resulting current $i_{Sabc}(t)$ is observed, reducing its THD from 13.45% to 2.77% with the fuzzy-SMC control compared to 0.99 obtained with the hysteresis control and 1.01 obtained with the sliding mode control.

Table VIII shows the THD of the panel current, the grid current and the resulting current $i_{Sabc}(t)$ before and after filtering obtained with the hysteresis, SMC and fuzzy-SMC correctors.

Figure 11. Waveforms of the PV generator, grid and resulting currents.

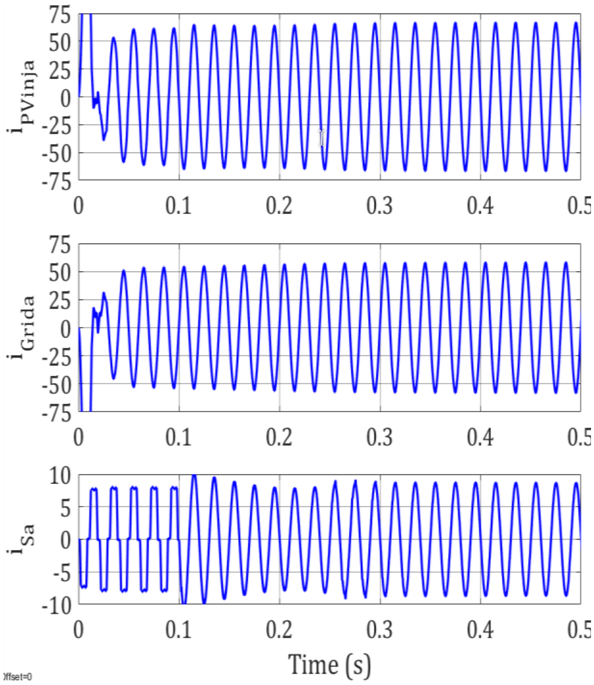


Figure 12. Waveforms of the load and filter currents

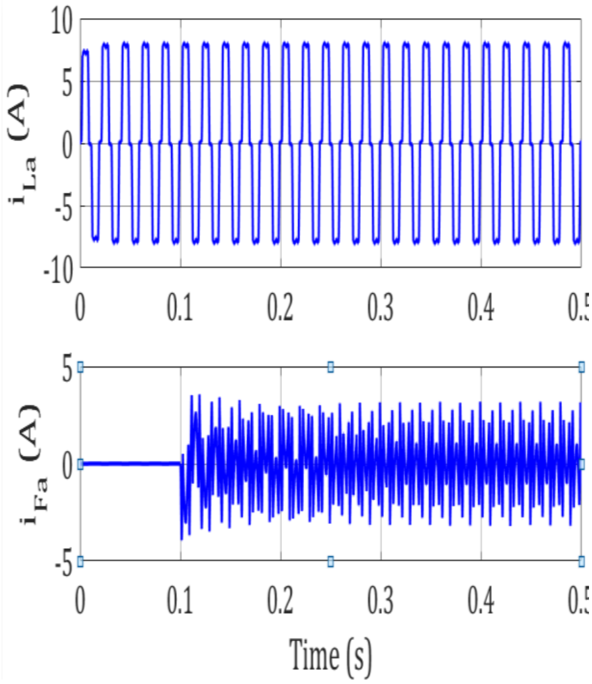


Figure 13. THDs of the PV generator, grid, resultant and load currents.

a. THD of the PV generator current

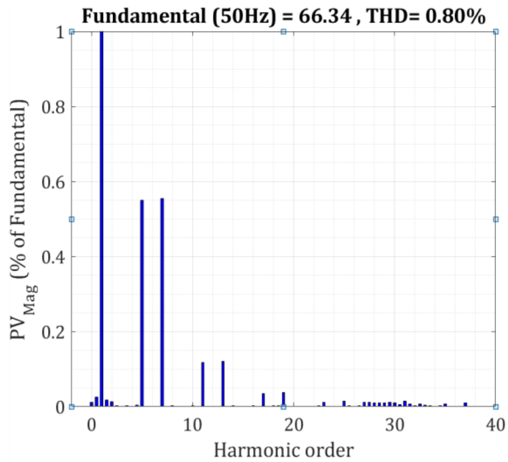


b. THD of the Grid current

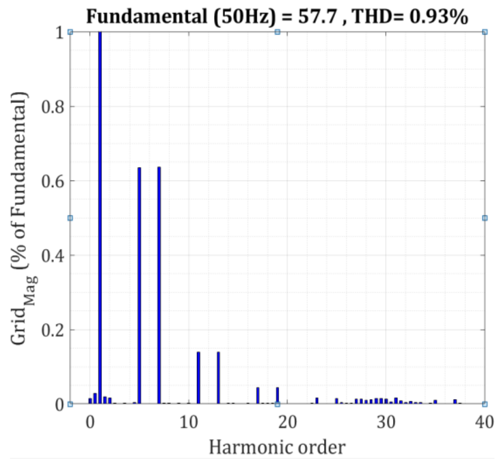

c. THD of the resulting current

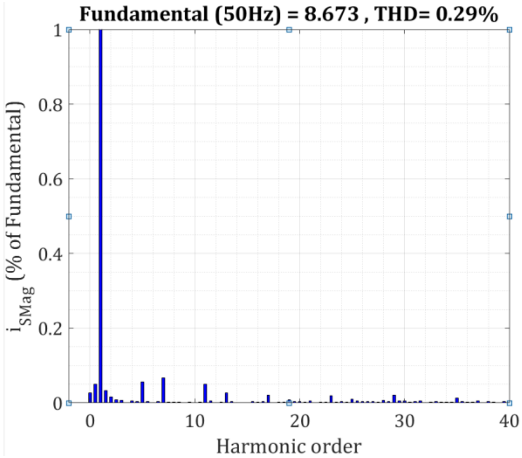


d. THD of the Load current

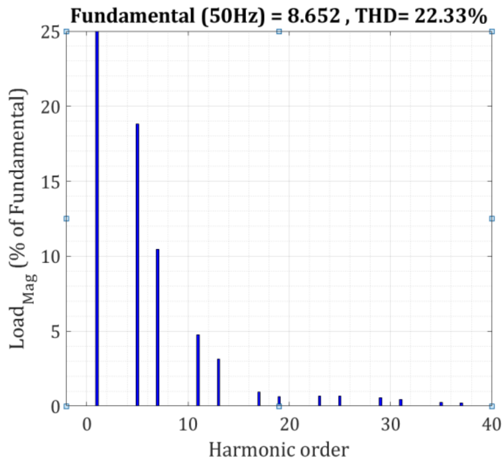


Figure 14. Waveforms of the PV generator, grid and resulting currents

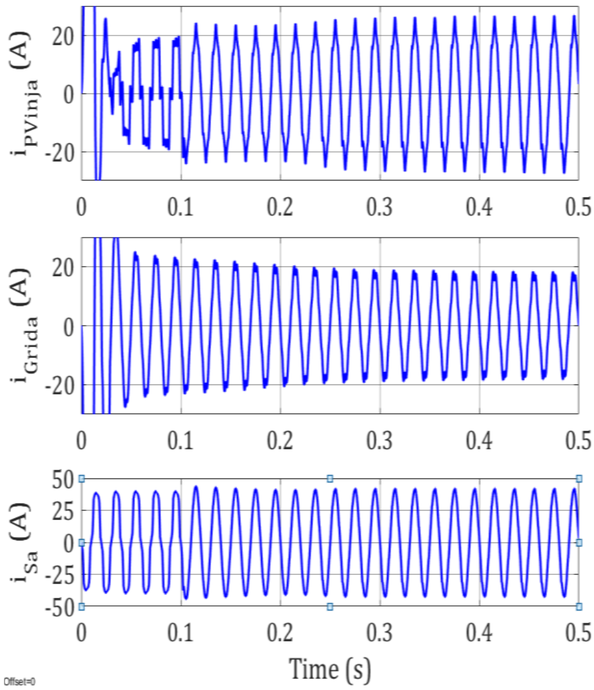


Figure 15. Waveforms of the load and filter currents

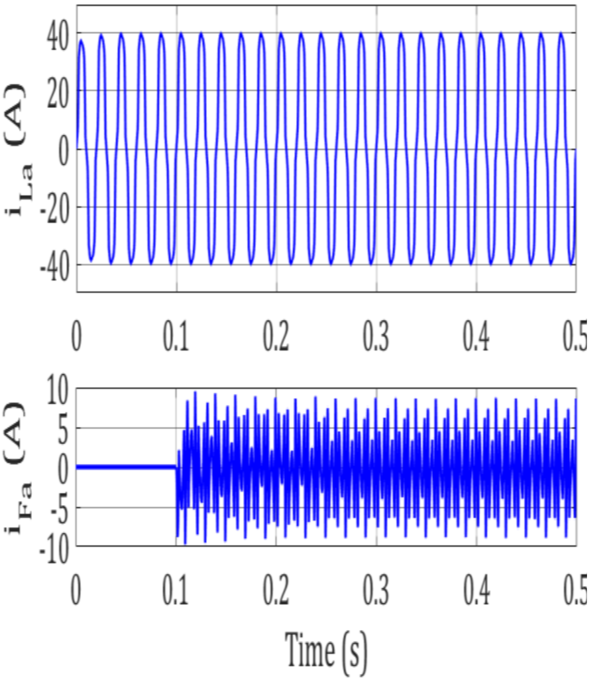


Figure 16.THDs of the PV generator, grid, resultant and load currents.

a. THD of the PV generator current

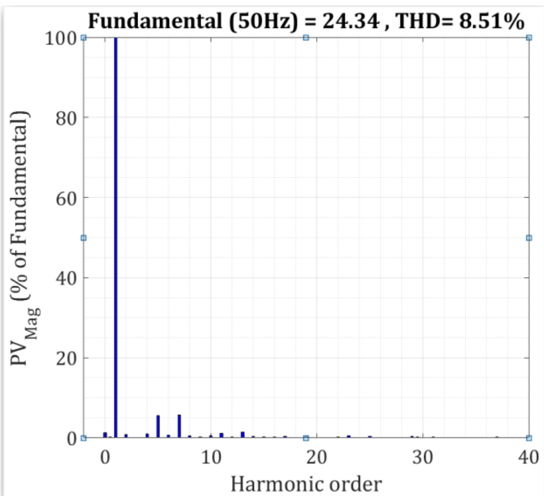


b. THD of the Grid current

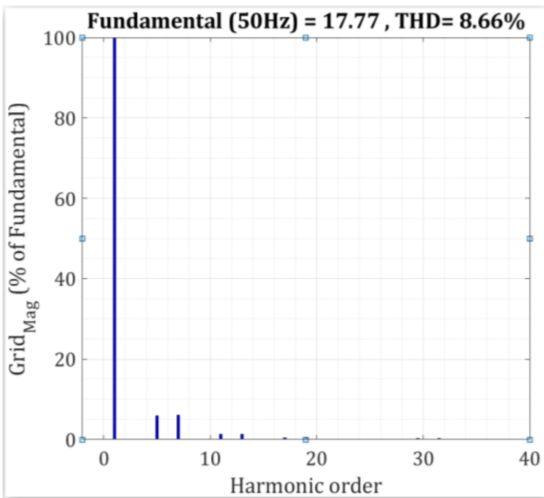

c. THD of the resulting current

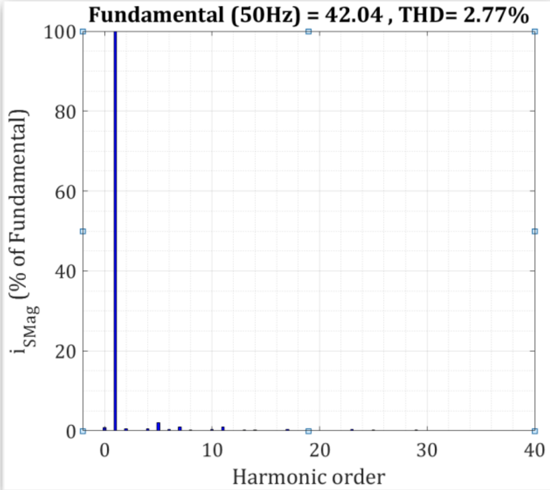


d. THD of the Load current

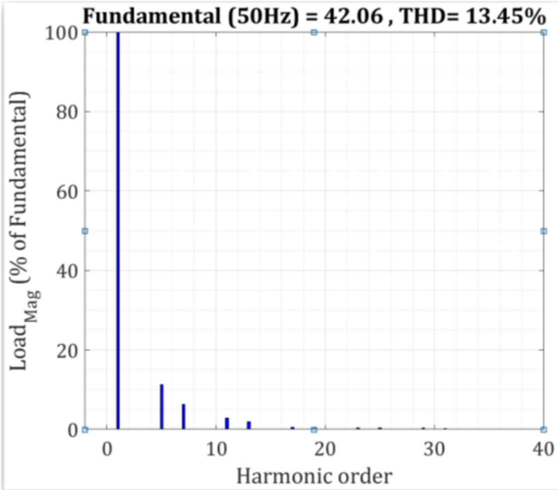


TABLE VIII. COMPARISON WITH SMC AND HYTHERESIS CONTROLLERS

| | | *Hysteresis* | *SMC* | *Fuzzy-SMC* |
|---|---|---|---|---|
| ***THD before filter*** | $i_{pv}$ | *32.09* | *32.09* | *32.09* |
| | $i_{Grid}$ | *6.87* | *6.87* | *6.87* |
| | $i_S$ | *13.45* | *13.45* | *13.45* |
| ***THD after filter*** | $i_{pv}$ | *8.25* | *8.28* | *8.51* |
| | $i_{Grid}$ | *8.65* | *8.67* | *8.66* |
| | $i_S$ | *3.50* | *3.00* | *2.77* |

## CONCLUSION

In this paper, the design of a fuzzy sliding mode controller is done for a shunt active power filter in order to reduce the harmonics in grid-connected photovoltaic system. The proposed control strategy consists of a sliding mode controller (SMC) and a fuzzy logic controller (FLC). The control law of the SMC is obtained from a sliding plane, thus cancelling the need to use the discontinuous component of the classical SMC. As the control laws obtained rely on the choice of constants, the FLC is used to determine these constants.The performance of SAPF in grid-connected PV system with the proposed controller was obtained by simulation on MATLAB/Simulink software. The results obtained show that the proposed controller allows to reduce the harmonics produced by the polluting load. In the case where the power of the PV generator is higher than that of the load, we obtain a THD of 0.29% for the current supplying the load after connection of the SAPF with the proposed controller compared to the 0.98% obtained with the SMC or the 0.95% obtained with the hysteresis. The current injected to the grid is of good quality with a THD of 0.93%.In the case where the power of the PV generator is lower than that of the load, although the current from the grid and the PV generator is highly distorted with THDs of 6.87% and 32.09% respectively before connecting the filter, the current obtained after filtering has a THD of 2.77% with the proposed controller.An implementation of the proposed controller on a FPGA or DSP board could be considered in future work for a study on a real system. In addition, a study of the behaviour of the controller in the event of network disconnection and reconnection during the operating scenario studied could be considered.

## REFERENCES

[1] M. Dali, J. Belhadj, and X. Roboam, "Hybrid solar–wind system with battery storage operating in grid-connected and standalone mode: Control and energy management – Experimental investigation," Energy, vol. 35, pp. 2587–2595, June2010.

[2] S. Kosai, and J. Cravioto, "Resilience of standalone hybrid renewable energy systems: The role of storage capacity," Energy, vol. 196, pp. 1–13, November 2020.

[3] U. Vargas, G. C. Lazaroiu, E. Tironi, and A. Ramirez, "Harmonic modeling and simulation of a stand-alone photovoltaic-battery-supercapacitor hybrid system," International Journal of Electrical Power & Energy Systems, vol. 105, pp. 70–78, February 2019.

[4] G.-H. Kim, C. Hwang, J.-H. Jeon, J.-B. Ahn, and E.-S. Kim, "A novel three-phase four-leg inverter based load unbalance compensator for stand-alone microgrid," International Journal of Electrical Power & Energy Systems, vol. 65, pp. 70–75, February 2015.

[5] P. Raseena, "Transformerless Photovoltaic Inverter for Standalone Scheme With Extended Input Voltage," Materials Today: Proceedings, vol. 24, pp. 1965–1971, 2020.

[6] K. A. Himali Lakshika, et al., "Reconfigurable solar photovoltaic systems: A review," Heliyon, vol. 6, pp. 1–18, April 2020.

[7] M. Parvez, M. F. M. Elias, N. A. Rahim, and N. Osman, "Current control techniques for three-phase grid interconnection of renewable power generation systems: A review," Solar Energy, vol. 135, pp. 29–42, October 2016.

[8] S. Ndjakomo Essiane, S. Perabi Ngoffe, A. Moukengue Imano, and L. Nneme Nneme, " Présentation et application d'un nouveau schéma de contrôle d'un filtre hybride parallèle à des réseaux électriques triphasés 400 V / 50 Hz et 480 V / 60 Hz," Afrique Science, vol. 10, pp. 27–38, May 2014.

[9] Y. Hoon, M. A. Mohd Radzi, M. K. Hassan, and N. F. Mailah, "Control algorithms of shunt active power filter for harmonics mitigations: a review," Energies, vol. 10, pp. 1–29, December 2017.

[10] Y. Hoon, M. A. Mohd Radzi, M. K. Hassan, and N. F. Mailah, "Enhanced instantaneous power theory with average algorithm for indirect current controlled three-level inverter-based shunt active power filter under dynamic state conditions," Mathematical Problems in Engineering, vol. 2016, pp. 1–12, February 2016.

[11] S. Adak, "Harmonics Mitigation of Stand-Alone Photovoltaic System Using LC Passive Filter," Journal of Electrical Engineering & Technology, vol. 16, pp. 2389–2396, May 2021.

[12] F. N. Belchior, L. R. de Lima, P. F. Ribeiro, and J. F. C. Castro, "A novel approach towards passive filter placement," In: Proceedings of 2015 IEEE power and energy society general meeting, Denver, USA, pp. 1–5, July 2015.

[13] Luis Moran, Juan Dixon, and Miguel Torres,Power Electronics Handbook, 4th ed., Butterworth-Heinemann, 2018, pp.1341–1379.

[14] M. Popescu, A. Bitoleanu, and V. Suru, "A DSP-based implementation of p-q theory in active power filtering under nonideal voltage conditions," IEEE Transactions on Industrial Informatics, vol. 9, pp. 880–889, May 2013.

[15] S. Adak, H. Cangi, B. Eid, and A. Serdar Yilmaz, "Developed analytical expression for current harmonic distortion of the PV system's inverter in relation to the solar irradiance and temperature," Electrical Engineering, vol. 103, pp. 697–704, 2021.

[16] S. R. N. Dzondé, H. Berviller, C. H. Kom, and P. Wira, "A unique FPGA for the implementation of neural strategies for identifying harmonic distortions," In: IECON 2013 - 39th Annual Conference of the IEEE Industrial Electronics Society, Vienna, Austria, pp. 352-357, November 2013.

[17] M. Monfared, S. Golestan, and J. M. Guerrero, "A new synchronous reference frame-based method for single-phase shunt active power filters," Journal of Power Electronics, vol. 13, pp. 692–700, July 2013.

[18] D. Chen, L. Xiao, W. Yan, Yan Li, and Y. Guo, "A harmonics detection method based on triangle orthogonal principle for shunt active power filter," Energy Reports, vol. 8, June 2021.

[19] E. Lavopa, P. Zanchetta, M. Sumner, and F. Cupertino, "Real-Time estimation of fundamental frequency and harmonics for active shunt power filters in aircraft electrical system," IEEE Transactions on Industrial Electronics, vol. 8, pp. 2875–2884, August 2009.

[20] O. Vodyakho, and C. C. Mi, "Tree-level inverter-based shunt active power flter in three-phase three-wire and four-wire systems," IEEE Transactions on Power Electronics, vol. 24, pp. 1350–1363, 2009.

[21] M. Karbasforooshan and M. Monfared, "An adaptive recursive discrete fourier transform technique for the reference current generation of single-phase shunt active power filters," In: 2016 7th Power Electronics and Drive Systems Technologies Conference (PEDSTC), Tehran, Iran, pp. 253–259, February 2016.

[22] A. T. Boum, G. B. Djidjio Keubeng, and L. Bitjoka, "Sliding mode control of a three-phase parallel active filter based on a two-level voltage converter," Systems Science & Control Engineering, vol. 5, pp. 535–543, November 2017.

[23] L. V. Assiene Mouodo, J. G. Tamba, O. T. Sosso Mayi, "H-Infinity Control of an Adaptive Hybrid Active Power Filter for Power Quality Compensation," Energy and Power Engineering, vol. 12, pp. 603–640, November 2020.

[24] R. Arun, B. Ramkiran, and Ayyapan, "Shunt active power filter using Hysteresis and PI control for improving the power quality using MATLAB," In: 2015 Online International Conference on Green Engineering and Technologies (IC-GET), Coimbatore, India, pp. 1–5, November 2015.

[25] A. A. Imam, R. Sreerama Kumar, and Y. A. Al-Turki, "Modeling and Simulation of a PI Controlled Shunt Active Power Filter for Power Quality Enhancement Based on P-Q Theory," Electronics, vol. 9, pp. 637, April 2020.

[26] S. Musa, M. A. M. Radzi, H. Hisham and N. I. Abdulwahab, "Fuzzy logic controller based three phase shunt active power filter for harmonics reduction," In: 2014 IEEE Conference on Energy Conversion (CENCON), Johor Bahru, Malaysia, pp. 371–376, October 2014.

[27] Agata Bielecka, and Daniel Wojciechowski, "Stability Analysis of Shunt Active Power Filter with Predictive Closed-Loop Control of Supply Current," Energies, vol. 14, pp. 1–17, April 2021.

[28] A. S. A. Hasim, Z. Ibrahim, S. M. F. S. M. Dardin, and J. Adnan, "The new technique of shunt active power filter employing Kalman filter estimator for photovoltaic grid-connected system," EnergiesIndian Journal of Science and Technology, vol. 9, pp. 1–8, December 2016.

[29] M. J. M. A. Rasul, H. V. Khang, and M. Kolhe, "Harmonic Mitigation of a Grid-connected Photovoltaic System using Shunt Active Filter," In: 2017 20th International Conference on Electrical Machines and Systems (ICEMS), Sydney, NSW, Australia, pp. 1–5, August 2017.

[30] M. A. Moftah, G. El-Saady, and E. A. Ibrahim, "Active power filter for power quality enhancement of photovoltaic renewable energy systems," In: 2016 Saudi Arabia Smart Grid (SASG), eddah, Saudi Arabia, pp. 1–9, December 2016.

[31] T. Louossi, N. Djongyang, O. T. Sosso Mayi, and A. Nanfak, "Perturb and observe maximum power point tracking method for photovoltaic systems using duty-cycle modulation," Journal of Renewable Energies, vol. 23, pp. 159–175, December 2020.

[32] J. K. Udavalakshmi, and M. S. Sheik, "Comparative Study of Perturb & Observe and Look-Up Table Maximum Power Point Tracking Techniques using MATLAB/Simulink," In: 2018 International Conference on Current Trends towards Converging Technologies (ICCTCT), Coimbatore, India, pp. 1–5, March 2018.

[33] F. E. Tahiri, K. Chikh, M. Khafallah, and A. Saad, "Comparative study between two Maximum Power Point Tracking techniques for photovoltaic system," In: 2016 International Conference on Electrical and Information Technologies (ICEIT), Tangiers, Morocco, pp. 107–112, May 2016.

[34] R. Kumar, B. Kumar and S. D., "Fuzzy Logic based Improved P&O MPPT Technique for Partial Shading Conditions," In: 2018 International Conference on Computing, Power and Communication Technologies (GUCON), Greater Noida, India, pp. 775–779, March 2019.

[35] L. Bouselham, B. Hajji and H. Hajji, "Comparative study of different MPPT methods for photovoltaic system," In: 2015 3rd International Renewable and Sustainable Energy Conference (IRSEC), Marrakech, Morocco, pp. 1–5, December 2015.

[36] M. J. P. Pesdjock, J. R. Mboupda Pone, D. Tchiotsop, M. R. Douanla, and G. Kenne, "Minimization of currents harmonics injected for grid connected photovoltaic systems using duty-cycle modulation technique," International Journal of Dynamics and Control, vol. 9, pp. 1013–1023, October 2020.

[37] N. Jaalam, N. A. Rahim, A. H. A. Bakar, ChiaKwang Tan, Ahmed M. A. Haidar, "A comprehensive review of synchronization methods for grid-connected converters of renewable energy source," Renewable and Sustainable Energy Reviews, vol. 59, pp. 1471–1481, June 2016.

[38] F. Biloa Assolo, C. H. Kom, A. Nanfak, and G. M. Ngaleu, "Harmonic pollution control of electrical networks: Comparative study of controls, by Pulse Width Modulation and by Duty Cycle Modulation of the three-phase shunt active Parallel filters," Journal of Electrical Engineering, Electronics, Control and Computer Science, vol. 7, pp. 41–52, July 2021.

[39] S. Kumaresan & H. Habeebullah Sait, "Design and control of shunt active power filter for power quality improvement of utility powered brushless DC motor drives," Automatika, vol. 61, pp. 507–521, June 2020

[40] H. Akagi, Y. Kanazawa, and A. Nabae, "Generalized Theory of the Instantaneous Reactive Power in Three-Phase Circuits," In: International Power Electronics Conference, Tokyo, Japan, pp. 1375–1386, 1983.

[41] M.-S. Karbasforooshan, M. Monfared, and M. Dogruel, "Indirect control of single-phase active power filters using harmonic control arrays," International Journal of Smart Electrical Engineering, vol. 5, pp. 185–190, June 2017

A. Štefek, V. T. Pham, V. Krivanek, and K. L. Pham, "Optimization of Fuzzy Logic Controller Used for a Differential Drive Wheeled Mobile Robot," Applied Sciences, vol. 11, pp. 1–23, June 2021.